Three Dimensional Wing Simulation by Panel Method with Tuned Wake Model

This report was made to fulfill as a final project assignment of

AE6000 Continuum Mechanics II

By:

Al-Faisal Firdaus 23621020

Rafael Stevenson 23621022

Advisor:

Dr. Lavi Rizki Zuhal

Aerospace Engineering Department

Faculty of Mechanical and Aerospace Engineering

Bandung Institute of Technology

2021

Contents

List of Figures

List of Tables

Chapter 1

Introduction

1.1 Background

The design process of aircraft's wing is very costly and time-consuming. In order to reduce the cost of it, numerical simulation can be utilized. One of the method that can be utilized is Viscous-Inviscid Interaction (VII). VII method divides the fluid domain into two parts, namely viscous domain and inviscid domain. Solutions of the invisicid domain outside of the viscous domain are computed by using Laplace equation and solutions of the viscous domain are computed by using Boundary Layer equations. In this report, the Laplace equation solver for inviscid domain will be further investigated.

In the inviscid region of the flow, the fluids are incompressible and irrotational. With the addition of steady-state assumption, the governing equation that governs the inviscid region will turn into laplace equation. Laplace equation is an elliptic differential equation, then the solution depends on the boundary conditions of the domain. In this research Panel method is utilized to solve the laplace equation. Panel Method uses linear combination of solutions from singularity element. In the panel method, wake modelling is

one of the crucial step to obtain an accurate result in the simulation. In this project, authors tested several wake modelling in the developed soruce code to solve flow around the wing using Panel Method.

1.2 Objectives

The objectives of this project are as

1. To Construct a panel method based solver program to solve pressure distribution around a three-dimensional wing and to obtain the aerodynamics force coefficients.

2. Perform an investigation on various kinds of wing study cases for the program's robustness.

3. Investigate what kind of wake model suits a particular case to obtain accurate results.

4. Study how accurate the proposed solver program is in various angle of attack conditions.

Chapter 2

Theoretical Background

2.1 The General Solution of Potential Flow

Given an incompressible and irrotational steady flow, the continuity equation of the flow is defined by the Laplace equation,

$$\nabla^2\phi = 0 \tag{2.1}$$

Consider a body with known boundaries S_B, submerged in a potential flow. The flow in region V in terms of the total potential Φ^* can be written using the continuity equation.

$$\nabla^2\Phi^* = 0 \tag{2.2}$$

Using Green's identity, one can construct equation 2.2 by a sum of source σ and doublet μ distributions placed on the boundary S_B. The total potential formula then become as follows.

$$\Phi^*(x,y,z) = \frac{-1}{4\pi}\int_{S_B}\left[\sigma\left(\frac{1}{r}\right) - \mu\mathbf{n}\cdot\nabla\left(\frac{1}{r}\right)\right]dS + \Phi_\infty \tag{2.3}$$

Here the vector $\mathbf{n}$ points in the normal direction of S_B and positive outside of V, and Φ_∞ is the free stream potential written as

$$\Phi_\infty = U_\infty x + V_\infty y + W_\infty z \tag{2.4}$$

In the general case of three-dimensional flows, specifying the boundary conditions will not immediately yield a unique solution. In order to make the solution unique, wake modelling have to be introduced to the geometry. Usually, the wake is modeled by thin double or vortex sheets, therefore equation 2.3 can rewritten into the following

$$\Phi^*(x,y,z) = \frac{1}{4\pi}\int_{\text{body+wake}} \mu\mathbf{n}\cdot\nabla\left(\frac{1}{r}\right)dS - \frac{1}{4\pi}\int_{\text{body}} \sigma\left(\frac{1}{r}\right)ds + \Phi_\infty \tag{2.5}$$

2.2 Singularity Elements

There are 2 types of singularity elements considered as boundary condition for solving equation 2.5. First singularity element is the point source σ. If a point element located at some $\mathbf{r}_0$, then the corresponding potential and velocity, expressed in Cartesian coordinates are as follows.

$$\Phi(x,y,z) = \frac{-\sigma}{4\pi\sqrt{(x-x_0)^2+(y-y_0)^2+(z-z_0)^2}} \tag{2.6}$$

$$\mathbf{u} = \left(\frac{\partial\Phi}{\partial x}, \frac{\partial\Phi}{\partial y}, \frac{\partial\Phi}{\partial z}\right) \tag{2.7}$$

Another singularity element is the point doublet. Using point doublet, the potential can be calculated as follows.

$$\Phi(x,y,z) = \frac{\mu}{4\pi}\begin{bmatrix}\frac{\partial}{\partial x}\\ \frac{\partial}{\partial y}\\ \frac{\partial}{\partial z}\end{bmatrix}\frac{1}{\sqrt{(x-x_0)^2+(y-y_0)^2+(z-z_0)^2}} \tag{2.8}$$

Similar to the point source, to get the velocity equation 2.8 must be integrated

2.2.1 Boundary Conditions

There are 3 boundary conditions that can be used to solve equation 2.2, mainly Neumann boundary condition ($\frac{\partial \Phi^*}{\partial n} = 0$ on the surface S_B), Dirichlet boundary condition (specied value of Φ^*), and mixed boudary condition. In this project, only Neumann and Dirichlet boundary are being utilized.

2.2.2 Neumann

In the Neumann boundary condition, the value of $\frac{\partial \Phi^*}{\partial n}$ will be specified on the solid boundary S_B. Therefore,

$$\nabla(\Phi + \Phi_\infty)\cdot = 0 \tag{2.9}$$

where Φ is the perturbation potential. To satisfy the boundary condition of equation 2.9 directly, one can use the velocity field due to the singularity distribution of equation 2.3

$$\nabla\Phi^*(P) = -\frac{1}{4\pi}\int_{Body}\sigma\nabla\left(\frac{1}{r}\right)dS + \frac{1}{4\pi}\int_{body+wake}\mu\nabla\left(\frac{\partial}{\partial n}\frac{1}{r}\right)dS + \Phi_\infty(P) \tag{2.10}$$

If the singularity distribution strengths σ and μ are known, then equation

2.10 describes the velocity field everywhere. Substituting equation 2.10 into boundary condition (equation 2.9) will results in the following equation.

$$\left\{ -\frac{1}{4\pi}\int_{Body}\sigma\nabla\left(\frac{1}{r}\right)dS + \frac{1}{4\pi}\int_{body+wake}\mu\nabla\left(\frac{\partial}{\partial n}\frac{1}{r}\right)dS + \Phi_\infty(P)\right\}\cdot n = 0 \tag{2.11}$$

2.2.3 Dirichlet

In the case of Dirichlet boundary condition, the perturbation potential Φ has to be specified everywhere on S_B. Using equation 2.3, and distributing the singularity elements on the surface, and placing the point (x, y, z) inside the surface S_B, the inner potential Φ^* can be calculated as follows.

$$\Phi^*(x,y,z) = \frac{1}{4\pi}\int_{body+wake}\left[\mu\frac{\partial}{\partial n}\left(\frac{1}{r}\right)\right]dS - \frac{1}{4\pi}\int_{Body}\left[\sigma\left(\frac{1}{r}\right)\right]dS + \Phi_\infty(P) \tag{2.12}$$

The velocity potential then becomes

$$\Phi^* = (\Phi + \Phi_\infty)_i = const \tag{2.13}$$

or

$$\Phi^*(x,y,z) = \frac{1}{4\pi}\int_{body+wake}\mu\frac{\partial}{\partial n}\left(\frac{1}{r}\right)dS - \frac{1}{4\pi}\int_{Body}\sigma\left(\frac{1}{r}\right)dS + \Phi_\infty(P) = const \tag{2.14}$$

If the velocity potential is defined differently, such as $\Phi^* = (\Phi + \Phi_\infty)_i = \Phi_\infty$, then equation 2.14 can be reduces to a simpler form as follows:

$$\frac{1}{4\pi}\int_{body+wake}\mu\nabla\left(\frac{\partial}{\partial n}\frac{1}{r}\right)dS-\frac{1}{4\pi}\int_{Body}\sigma\nabla\left(\frac{1}{r}\right)dS=0 \tag{2.15}$$

Consequently, the above equation is based on the fact that if Neumann boundary condition is equivalent to

$$\frac{\partial\Phi}{\partial n}=-n\cdot Q_\infty \tag{2.16}$$

Using the definition of $-\sigma=\dfrac{\partial\Phi^*}{\partial n}-\dfrac{\partial\Phi_i^*}{\partial n}$, and boundary conditions, one will get the source strength is required to be

$$\sigma=n\cdot Q_\infty \tag{2.17}$$

2.3 Wake Model

Wake modelling is important in the solving of potential flow. The wake will make the obtained solution of the potential flow unique. In the modelling of the wake there are 2 things that must be considered: The wake strength at the trailing edge and the wake shape.

The simplest solution regarding the definition of the wake strength is to apply the two-dimensional Kutta condition along the wing trailing edge ($\gamma_{TE}=0$). Rewriting the Kutta condition in terms of the doublet strength, one can get the following equation.

$$\mu_{\text{upper surface}}-\mu_{\text{lower surface}}-\mu_{\text{wake}}=0 \tag{2.18}$$

Similarly, in terms of the circulation Γ, one can get as follows

$$\Gamma_{\text{wake}} = \Gamma_{\text{upper surface}} - \Gamma_{\text{lower surface}} \tag{2.19}$$

On the wake shape in three dimensions, the wake influence is more dominant and thus its geometry affects the solution considerably. Recall the formulation for a force $\nabla\mathbf{F}$ generated by a vortex sheet γ. .

$$\Delta F = \rho \mathbf{q} \times \gamma \tag{2.20}$$

In the three dimensional case, the value of $\delta\mathbf{F}$ must be 0 when the local flow is parallel to the γ. Therefore, one can use the following condition for the wake geometry.

$$\mathbf{q} \times \gamma_{\text{wake}} = 0 \tag{2.21}$$

Similarly, for a wake represented by a thin doublet sheet,

$$\mathbf{q} \times \mu_{\text{wake}} = 0 \tag{2.22}$$

Therefore, the condition required for the wake panels, in terms of doublets is as follows.

$$\mu_{\text{wake}} = constant \tag{2.23}$$

The difficulty in satisfying this condition is that the wake location is not known at first. Therefore, several wake model could be used to increased the accuracy of the calculation.

Chapter 3

Numerical Algorithm

3.1 Program Structure

In this chapter, the numerical algorithm of the 3-Dimensional potential solver for wing will be further elaborated. The flowchart of the developed program for this project is shown in figure 3.1 .

The first two steps are loading airfoil data and creating the 3D wing model and wake. In the developed program, the airfoil geometry will be modified so that the trailing edge will always be closed. In the wing generation, several parameters, such as free-stream velocity, wing span, root chord, tip chord, etc, are all following the users input. At the same time, the geometry definition was implemented by creating grid at the wing surface. The discretization is controlled by determining the number of span-wise panels and airfoil coordinate points. For the wake modelling, the user can input how many grids divider needed for the grids generated at wake. Overall, only half-wing configuration is made, it is to avoid more computational time in making the 3 dimensional model.

The next step is calculating the strength of source and doublet at each

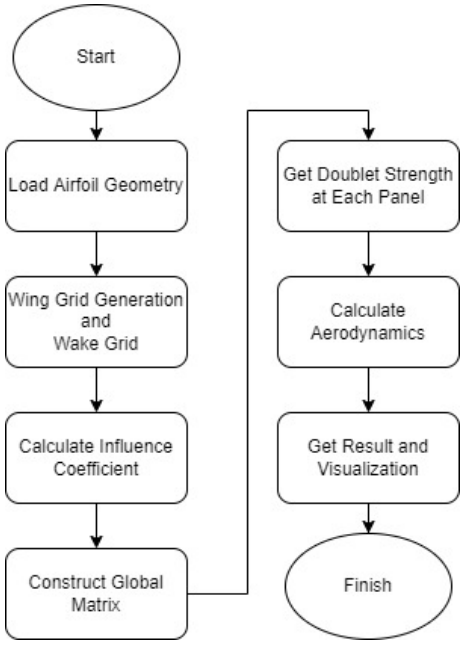

Figure 3.1: Program Flowchart

panel. Calculating the velocity from the integral form of source and doublet was quite complicated. The implementation was divided into two parts because of the summation of each panel were done on its own local coordinates. First, local frame of reference of each panel was calculated, then the results will be used to calculate the influence parameter of source and doublet. The velocity of each panel can be calculated using the summation of the influence parameters. To fulfill the boundary condition, which is normal velocity at panel must be zero, all of the boundary condition equations were constructed to a global matrix. The global matrix will be solver to obtain the doublet strength of each panel. Additional boundary condition is added to the global matrix which is the Kutta condition at the trailing edge of the wing. This was done to ensure the flow at trailing edge parallel to the airfoil and the solution is unique.

The last step is to calculate the aerodynamics parameters: pressure co-

efficient (C_p), lift coefficient (C_L), and moment coefficient (C_m). The drag calculation is not yet available because in this project the viscous effect of the simulation is neglected. The post-processing is done using Paraview and several data are plotted using Matplotlib library in Python.

3.2 Grid Generation

The grid was made on the wing surface as panels. The coordinate is defined following REF where x-axis is the chordwise direction, y-axis is the span-wise direction, and z-axis is the direction from the cross product between x and y axis. This will be the main simulation coordinate used in the simulation. In the computation domain, the grid points were stored in array containing (x, y, z) values.

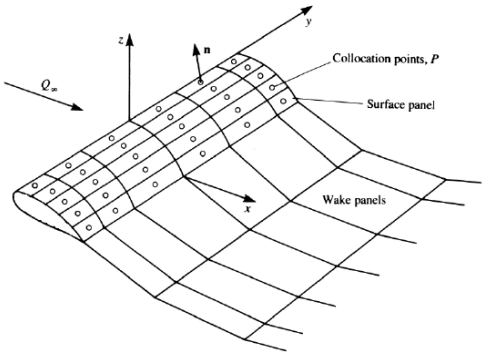

Figure 3.2: Grid panels along wing surface and wake [1]

There were several types of grids point stored while calculating the solution of potential flow. First, the corner point at each panel. Four corner points will be used to construct a panel. Second, the collocation point at each point. The collocation point is located at the center of each panel and calculated by averaging from 4 corner points that constructed a panel. The

visualization of the grid in the wing and the used points are shown in figure 3.3

On the other hand, grid generation for the wake in the Authors program is done by dividing panels using user input criteria, namely wake divider. The wake divider is only dividing the wake panels in the x-axis direction. For the y-axis divider, it will follows the total number of spanwise panels. The better visualization of the wake can also be seen in figure 3.3.

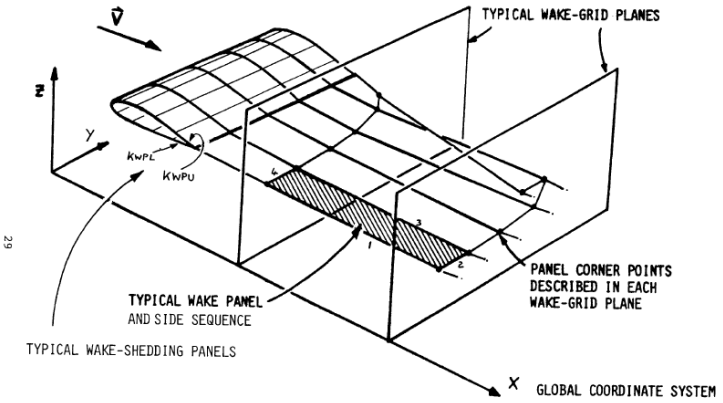

Figure 3.3: Wake grid scheme [2]

3.3 Aerodynamic Calculation

This section will discuss about the process of obtaining the strength of source and doublet at each panel such that the numerical approximation meets the physical boundary condition requirements. The formulation is done following reference [1] and Dirichlet boundary condition was chosen for the developed program.

The integration of equation 2.14 becomes more convenient if the calculation was done in the local frame of reference at each panel. Therefore, the

influence calculation and global matrix construction will be done using the local frame of reference of each panels. The collocation point (center point at a panel) will be also constructed using the local frame of reference, therefore it will be unique for each panel.

3.3.1 Influence

The influence coefficient is calculated using quadrilateral constant source or doublet to a target panel collocation point as can be seen in figure 3.4. this procedure is repeated for each pair of panels to obtain all of panels influence coefficient.

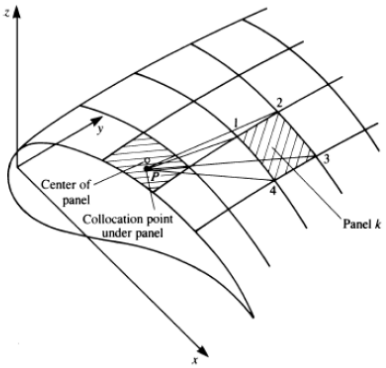

Figure 3.4: Schematic of influence calculation

For a quadrilateral constant strength source in the local coordinate frame, the equation of velocity potential is given as follows,

$$\Phi_s(x, y, z) = \frac{-\sigma}{4\pi} \int_S \frac{dS}{\sqrt{(x - x_o)^2 + (y - y_o)^2} + z^2} \tag{3.1}$$

where x_o and y_o is the center of local coordinate (collocation point). Execution of the integration within the area bounded by the four straight lines requires a lengthy process and is derived by Hess and Smith [3]. Using their

results, one can obtain the potential for a planar element as

$$\begin{aligned}\Phi_s(x,y,z) = \frac{-\sigma}{4\pi}\Bigg\{\Bigg[&\frac{(x-x_1)(y_2-y_1)-(y-y_1)(x_2-x_1)}{d_{12}}\ln\left(\frac{r_1+r_2+d_{12}}{r_1+r_2-d_{12}}\right)\\ &+\frac{(x-x_2)(y_3-y_2)-(y-y_2)(x_3-x_2)}{d_{23}}\ln\left(\frac{r_2+r_3+d_{23}}{r_2+r_3-d_{23}}\right)\\ &+\frac{(x-x_3)(y_4-y_3)-(y-y_3)(x_4-x_3)}{d_{34}}\ln\left(\frac{r_3+r_4+d_{34}}{r_3+r_4-d_{34}}\right)\\ &+\frac{(x-x_4)(y_1-y_4)-(y-y_4)(x_1-x_4)}{d_{41}}\ln\left(\frac{r_4+r_1+d_{41}}{r_4+r_1-d_{41}}\right)\Bigg]\\ &-|z|\Bigg[\tan^{-1}\left(\frac{m_{12}e_1-h_1}{zr_1}\right)-\tan^{-1}\left(\frac{m_{12}e_2-h_2}{zr_2}\right)\\ &+\tan^{-1}\left(\frac{m_{23}e_2-h_2}{zr_2}\right)-\tan^{-1}\left(\frac{m_{23}e_3-h_3}{zr_3}\right)\\ &+\tan^{-1}\left(\frac{m_{34}e_3-h_3}{zr_3}\right)-\tan^{-1}\left(\frac{m_{34}e_4-h_4}{zr_4}\right)\\ &+\tan^{-1}\left(\frac{m_{41}e_4-h_4}{zr_4}\right)-\tan^{-1}\left(\frac{m_{41}e_1-h_1}{zr_1}\right)\Bigg]\Bigg\}\end{aligned} \tag{3.2}$$

where

$$\begin{aligned} d_{ij} &= \sqrt{(x_j-x_i)^2+(y_j-y_i)^2}\\ m_{ij} &= \frac{y_j-y_i}{x_j-x_i}\\ r_k &= \sqrt{(x-x_k)^2+(y-y_k)^2+z^2}\\ e_k &= (x-x_k)^2+z^2\\ h_k &= (x-x_k)(y-y_k)\end{aligned} \tag{3.3}$$

All of the elements in equation 3.2 except the source strength is the influence coefficient from constant source (B_k) in the quadrilateral panel to some certain point (x, y, z). In the simulation of wing, the point will be the collocation point of other panels.

For the quadrilateral constant strength doublet (μ), the equation can be seen in equation 3.4.

$$\Phi_d(x,y,z) = \frac{-\mu}{4\pi}\int_S \frac{z dS}{[(x-x_o)^2+(y-y_0)^2+z^2]^{\frac{3}{2}}} \tag{3.4}$$

Following Hess and Smith [3], one can get the following formula for quadrilateral constant strength doublet.

$$\begin{aligned}\Phi_d(x,y,z) = \frac{\mu}{4\pi}\Bigg[&\tan^{-1}\left(\frac{m_{12}e_1-h_1}{zr_1}\right)-\tan^{-1}\left(\frac{m_{12}e_2-h_2}{zr_2}\right)\\ &+\tan^{-1}\left(\frac{m_{23}e_1-h_2}{zr_2}\right)-\tan^{-1}\left(\frac{m_{23}e_3-h_2}{zr_3}\right)\\ &+\tan^{-1}\left(\frac{m_{34}e_3-h_3}{zr_3}\right)-\tan^{-1}\left(\frac{m_{34}e_4-h_4}{zr_4}\right)\\ &+\tan^{-1}\left(\frac{m_{41}e_4-h_4}{zr_4}\right)-\tan^{-1}\left(\frac{m_{41}e_1-h_1}{zr_1}\right)\Bigg]\end{aligned} \tag{3.5}$$

The simulation was done only for half wing span, therefore during calculation of the influence coefficient the contribution from the image panel should be added.

3.3.2 Trailing Edge Condition

After calculating all the influence coefficients, the global matrix will be constructed. To fulfill the boundary condition, one must add the condition at the wing trailing edge and the wake which has been mentioned in the Chapter 2. This trailing edge condition can be seen in figure xx

The conditions for the additional boundary is as follows: if the panel is not at the trailing edge, only doublet influence exist, and if the panel is at the trailing edge, the doublet influence must be added/subtracted with wake

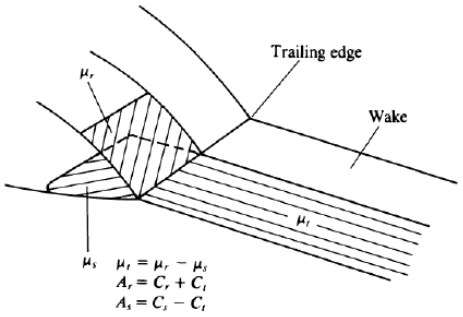

Figure 3.5: Trailing edge condition

influence (C_t). Therefore, the additional condition can be written mathematically.

$$\begin{aligned} A_k &= C_k, \text{ if panel is not at trailing edge} \\ A_k &= C_k \pm C_t, \text{ if panel is at trailing edge} \end{aligned} \tag{3.6}$$

The Kutta-condition is combined inside the global matrix without adding additional row to the global matrix. It is represented by the coefficient A_k for panels in panels at trailing edge.

3.3.3 Global Matrix Construction

The global matrix construction is based on equation 2.15. Before constructing the global matrix, equation 2.15 should be simplified using parameters A_k and B_k for each collocation point in the simulation. Therefore the simplified equation can be written as follows.

$$\sum_{k=1}^{N} A_k \mu_k + \sum_{k=1}^{N} B_k \sigma_k = 0 \tag{3.7}$$

The source strength is already known, therefore the summation of source strength can be move to the right hand side of the equation.

$$\sum_{k=1}^{N} A_k \mu_k = -\sum_{k=1}^{N} B_k \sigma_k \tag{3.8}$$

For N collocation points in the computation domain, equation 3.8 becomes N equations with N unknowns μ. The matrix system is as follows

$$\begin{pmatrix} A_{11} & A_{12} & \cdots & A_{1N} \\ A_{21} & A_{22} & \cdots & A_{2N} \\ \vdots & \vdots & \ddots & \vdots \\ A_{N1} & A_{N2} & \cdots & A_{NN} \end{pmatrix} \begin{pmatrix} \mu_1 \\ \mu_2 \\ \vdots \\ \mu_N \end{pmatrix} = - \begin{pmatrix} B_{11} & B_{12} & \cdots & B_{1N} \\ B_{21} & B_{22} & \cdots & B_{2N} \\ \vdots & \vdots & \ddots & \vdots \\ B_{N1} & B_{N2} & \cdots & B_{NN} \end{pmatrix} \begin{pmatrix} \sigma_1 \\ \sigma_2 \\ \vdots \\ \sigma_N \end{pmatrix} \tag{3.9}$$

The right hand side is the source terms and can be rewritten as RHS. Therefore, the final matrix equation is as follows.

$$\begin{pmatrix} A_{11} & A_{12} & \cdots & A_{1N} \\ A_{21} & A_{22} & \cdots & A_{2N} \\ \vdots & \vdots & \ddots & \vdots \\ A_{N1} & A_{N2} & \cdots & A_{NN} \end{pmatrix} \begin{pmatrix} \mu_1 \\ \mu_2 \\ \vdots \\ \mu_N \end{pmatrix} = \begin{pmatrix} RHS_1 \\ RHS_2 \\ \vdots \\ RHS_N \end{pmatrix} \tag{3.10}$$

3.4 Aerodynamic Force Calculation

The aerodynamic force can be calculated using doublet strength, source strength, and free stream velocity potential. From these information, the pressure coefficient C_p for each panel could be calculated. After that, the coefficient of lift C_L and coefficient of moment C_M could be computed using the value of C_p.

In panel coordinate, each panel perturbation velocity (q) could be calculated using equation xx. In numerical approach, finite difference was used to

calculate the derivatives.

The total velocity (Q) is defined as follows

$$\mathbf{Q} = \mathbf{Q}_\infty + \mathbf{q} \tag{3.11}$$

where $textbf{Q}_\infty$ is the free stream velocity and $\mathbf{q}$ is the perturbation velocity. Using the panel coordinate (l, m, n), equation 3.11 could be rewritten in the vector form as follows.

$$\mathbf{Q} = (Q_{\infty,l} + ql, Q_{\infty,m} + qm, Q_{\infty,n} + qn) \tag{3.12}$$

The pressure coefficient C_p can be calculated using the following equation.

$$C_{p,k} = 1 - \frac{Q_k^2}{Q_\infty^2} \tag{3.13}$$

The pressure force always pointed to the negative normal direction of the panels, thus to get lift force the pressure force should be projected (in local panel coordinate). To get the force contribution of a certain panel, the pressure coefficient must be multiplied by the panel surface area. Then by doing the summation for all the panels, one could obtain the lift force. Note that the simulation is just half wing, so the force calculated is just half from the actual force. The Coefficient of lift and moment is formulated as follows

$$C_L = \frac{\sum_{k=1}^{N}(C_{p,k}\Delta S_k r_L)}{(\frac{C_R+C_T}{2})(\frac{b}{2})} \tag{3.14}$$

$$C_M = \frac{\sum_{k=1}^{N}(C_{p,k}\Delta S_k r_L x_k)}{(\frac{C_R+C_T}{2})(\frac{b}{2})C_m} \tag{3.15}$$

where r_L is the rotation factor from normal in local coordinate to normal to free stream direction. C_R and C_T are root chord and root tip. In the

moment calculation, the lift force is multiplied by the moment arm (x_k) and the result will be divided by mean chord (C_m).

3.5 Study Cases

This work will consider two kinds of study cases where the first study case would be a wing that has a cambered airfoil with a small sweep, but as for the second case the wing will use a symmetrical airfoil and the wing has now sweep. The details of both cases are:

1. Cambered Airfoil Wing
    - Airfoil: NACA 4412
    - Root Chord: 1.0 m
    - Tip Chord: 0.8 m
    - Aft Sweep of Tip: 0.1 m
    - Wing Span: 10.0 m
    - Free Stream Velocity: 1 m/s
2. Symmetrical Airfoil Wing
    - Airfoil: NACA 0010
    - Root Chord: 1.0 m
    - Tip Chord: 0.8 m
    - Aft Sweep of Tip: 0.0 m
    - Wing Span: 10.0 m
    - Free Stream Velocity: 1 m/s

3.6 Wake Model Types

The analyses in this work will also investigate how the wake model could actually affect the accuracy of the panel method solver. There would be 5 types of wake models defined namely wake model 1 to 5 where wake model 1 is the upper side extreme where it has a positive angle at the counter-clockwise direction against the horizontal axis and the wake model 5 is the lower side extreme where it has a negative angle from the same reference with wake model 1 and wake model 2, 3, and 4 will be in between 1 and 5 as shown in the figure below where wake model 3 would be at a zero angle against the horizontal axis. Also later on, the angle of wake model 1 and 5 will depend on the angle of attack at that case where the angle that the wake model 1 and 5 has against the horizontal axis is the same as the angle of attack at that particular case and wake model 2 and 4 will be half of that value in the direction. So, as for example if the angle of attack (AoA) is 3°, wake model 1 and 5 will be at 3° and wake model 2 and 4 will be at 1.5° against the horizontal axis in opposing directions as shown in the figure below.

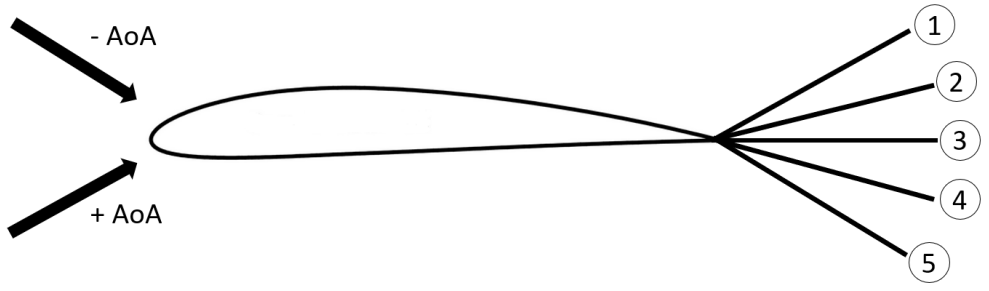

Figure 3.6: Angle of attack and the wake model variations

Chapter 4

Results and Analysis

4.1 Mesh Convergence

Before we perform calculations and analyze the program's results compared to the benchmark results generated from XFLR5 software, a mesh convergence test was performed for both cases where this aims to inform the number of panels required to properly capture consistent result from the solver where more panels will have a more detailed and accurate solutions to capture the physics involved but using too many panels will require larger computational power and time. Therefore, it is important to ensure that the result is already consistent and we do not use too many panels. The mesh convergence test was performed both for the proposed solver and the XFLR5 solver where eventually the same number of mesh for both solver would be used to compare results.

4.1.1 Cambered Airfoil Case

The mesh convergence test performed for the first case with cambered airfoil case of wing with NACA 4412 airfoil for the panel method solver are as

shown below.

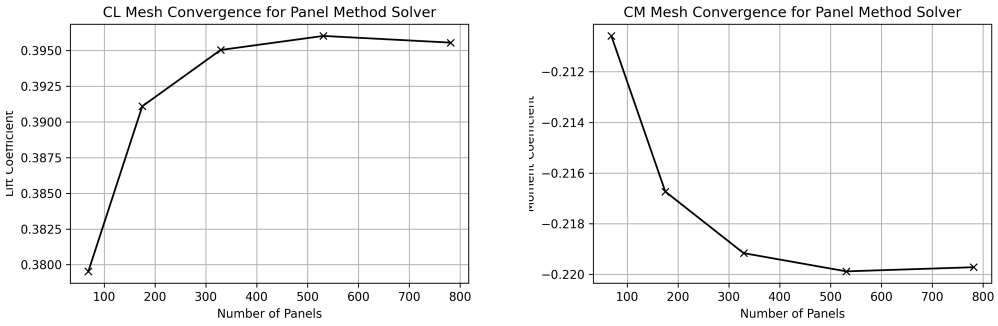

(a) (b)

Figure 4.1: Cambered case panel method solver (a) CL convergence, (b) CM convergence

Also, the mesh convergence test for the XFLR5 solver are as shown below.

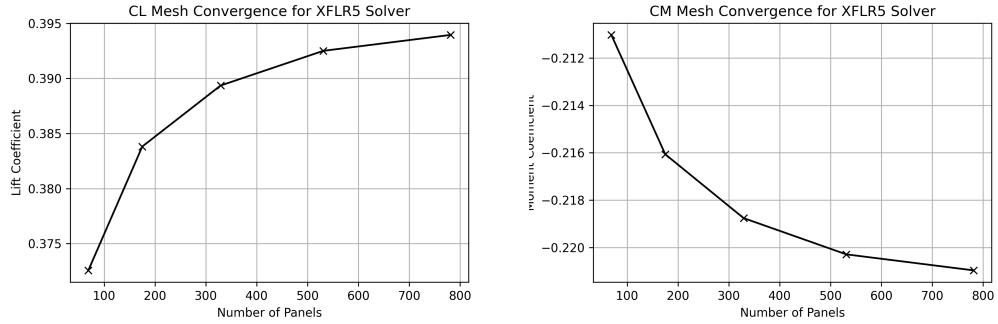

(a) (b)

Figure 4.2: Cambered case XFLR5 solver (a) CL convergence, (b) CM convergence

The detailed number of panels and the computation time for the panel method solver are as shown below.

Table 4.1: Cambered case number of panels variation

Chordwise Panels	Spanwise Panels	Wake Divider	Total Panels	Runtime (s)
20	3	3	69	1.842
30	5	5	175	9.929
40	7	7	329	33.208
50	9	9	531	88.564
60	11	11	781	188.589

The number of panels eventually taken is the total panels of 781 where it is already a convergent mesh for the panel method solver and the XFLR5 solver.

4.1.2 Symmetrical Airfoil Case

Similarly the mesh convergence test was also performed for the second case with symmetrical airfoil case of wing with NACA 0010 airfoil for the panel method solver are as shown below.

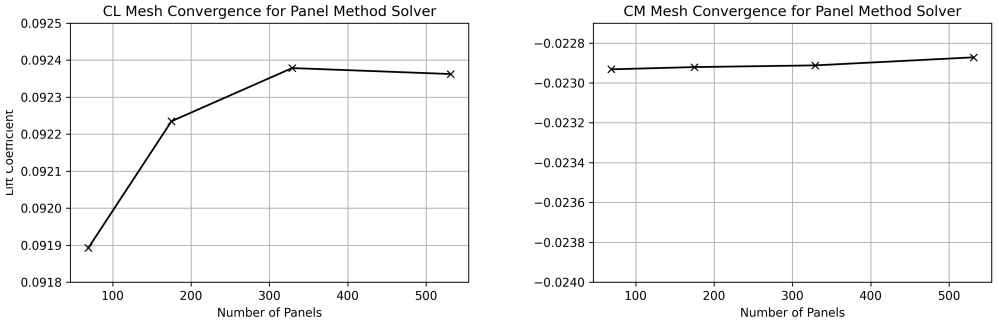

(a) (b)

Figure 4.3: Symmetrical case panel method solver (a) CL convergence, (b) CM convergence

Also, the mesh convergence test for the XFLR5 solver are as shown below.

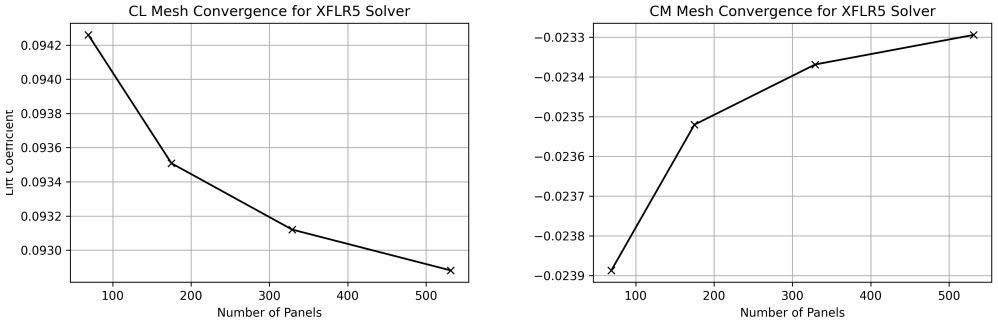

(a) (b)

Figure 4.4: Symmetrical case XFLR5 solver (a) CL convergence, (b) CM convergence

The detailed number of panels and the computation time for the panel method solver are as shown below.

Table 4.2: Symmetrical case number of panels variation

Chordwise Panels	Spanwise Panels	Wake Divider	Total Panels	Runtime (s)
20	3	3	69	1.826
30	5	5	175	9.269
40	7	7	329	32.049
50	9	9	531	86.311

The number of panels eventually taken is the total panels of 531 where it is already a convergent mesh for the panel method solver and the XFLR5 solver.

4.2 Post-Processing Results

This section will provide an example of how the grid generation and pressure coefficients distribution results are. The Results presented in this section is only for the case with number of panels that has been selected in the

previous section by the mesh convergence test. The grid generation results can be seen in figure 4.5(a) and (b). Additionally, the pressure coefficient distribution results can be seen in figure 4.6(a) and (b).

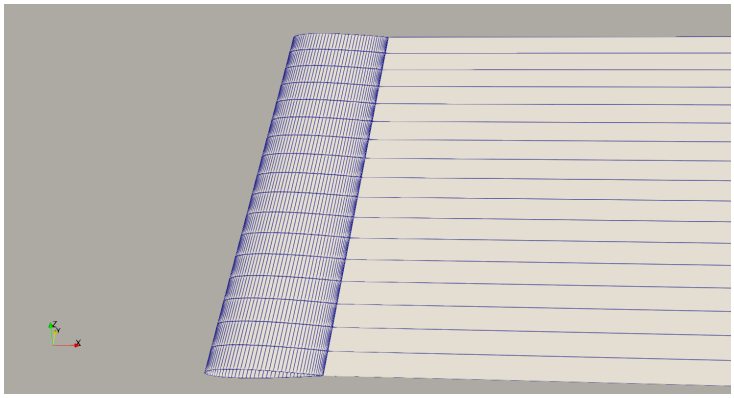

(a)

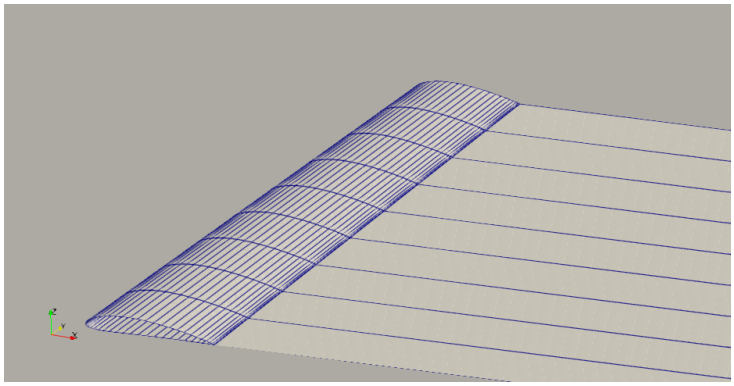

(b)

Figure 4.5: The resulting panels from grid generation solver for (a) NACA 4412, (b) NACA 0010

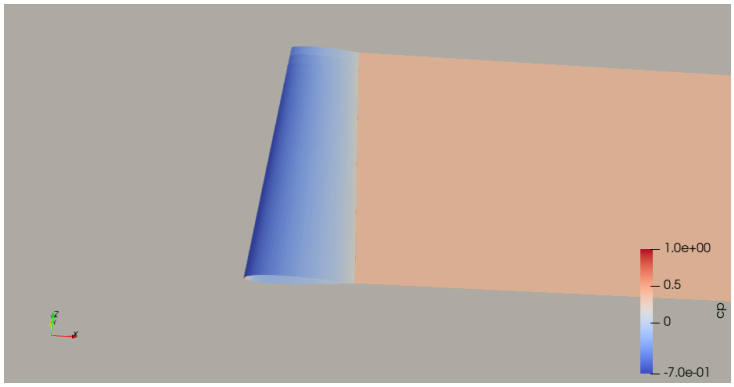

(a)

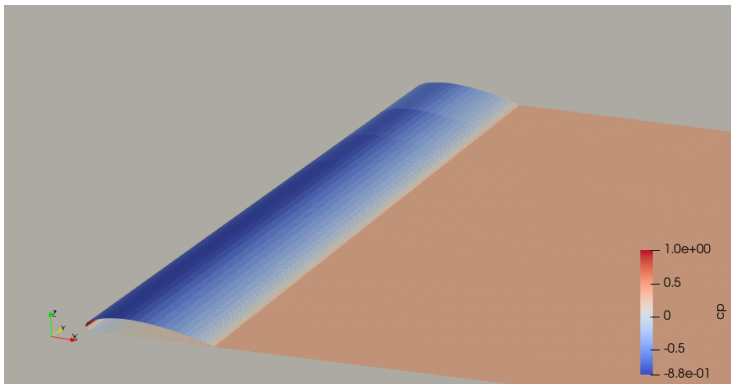

(b)

Figure 4.6: The resulting pressure coefficients for (a) NACA 4412, (b) NACA 0010

From the figures, the results show that the grid generation solver is capable of producing computational panels as intended. The C_p distribution results are presented to showcase the results of the simulation. The detailed study of the simulation results will be discussed in the following sections.

4.3 Wake Model Variations

As previously described, this work investigates how different kinds of wake model variations affect the obtained results. Therefore this section will focus on analyzing and identifying what kind of wake model is appropriate to

obtain a better result from the panel method solver compared to the XFLR5 solver.

4.3.1 Cambered Airfoil Case

This section presents the results of the panel method solver in a variety of wake models as described in chapter 3 for the cambered airfoil case compared to the XFLR5 solver.The results for the -1˚to 3˚angle of attack varied by the wake models respectively are as

Table 4.3: Cambered case AoA -1° wake variation results

Wake Model	Panel Method Solver		XFLR5 Solver		Error Percentage		
	CL	CM	CL	CM	CL Error %	CM Error %	Averaged Error %
1	0.30258	-0.19212	0.30053	-0.19261	0.68277	0.25427	0.46852
2	0.30253	-0.19210	0.30053	-0.19261	0.66776	0.26784	0.46780
3	0.30249	-0.19207	0.30053	-0.19261	0.65369	0.28084	0.46727
4	0.30245	-0.19205	0.30053	-0.19261	0.64058	0.29326	0.46692
5	0.30242	-0.19203	0.30053	-0.19261	0.62843	0.30511	0.46677

Table 4.4: Cambered case AoA 0° wake variation results

Wake Model	Panel Method Solver		XFLR5 Solver		Error Percentage		
	CL	CM	CL	CM	CL Error %	CM Error %	Averaged Error %
1	0.39568	-0.21979	0.39395	-0.22096	0.43864	0.53021	0.48443
2	0.39562	-0.21975	0.39395	-0.22096	0.42227	0.54654	0.48440
3	0.39556	-0.21972	0.39395	-0.22096	0.40685	0.56221	0.48453
4	0.39550	-0.21969	0.39395	-0.22096	0.39239	0.57722	0.48481
5	0.39545	-0.21965	0.39395	-0.22096	0.37888	0.59158	0.48523

Table 4.5: Cambered case AoA 1° wake variation results

Wake Model	Panel Method Solver		XFLR5 Solver		Error Percentage		
	CL	CM	CL	CM	CL Error %	CM Error %	Averaged Error %
1	0.48860	-0.24736	0.48719	-0.24926	0.28942	0.75996	0.52469
2	0.48851	-0.24732	0.48719	-0.24926	0.27169	0.77877	0.52523
3	0.48843	-0.24727	0.48719	-0.24926	0.25491	0.79685	0.52588
4	0.48835	-0.24723	0.48719	-0.24926	0.23908	0.81422	0.52665
5	0.48828	-0.24719	0.48719	-0.24926	0.22421	0.83086	0.52754

Table 4.6: Cambered case AoA 2° wake variation results

Wake Model	Panel Method Solver		XFLR5 Solver		Error Percentage		
	CL	CM	CL	CM	CL Error %	CM Error %	Averaged Error %
1	0.58145	-0.27494	0.58018	-0.27747	0.22004	0.91312	0.56658
2	0.58121	-0.27481	0.58018	-0.27747	0.17898	0.95761	0.56830
3	0.58100	-0.27470	0.58018	-0.27747	0.14174	0.99901	0.57038
4	0.58080	-0.27459	0.58018	-0.27747	0.10832	1.03734	0.57283
5	0.58063	-0.27449	0.58018	-0.27747	0.07871	1.07259	0.57565

Table 4.7: Cambered case AoA 3° wake variation results

Wake Model	Panel Method Solver		XFLR5 Solver		Error Percentage		
	CL	CM	CL	CM	CL Error %	CM Error %	Averaged Error %
1	0.67403	-0.30241	0.67286	-0.30556	0.17373	1.03099	0.60236
2	0.67356	-0.30217	0.67286	-0.30556	0.10375	1.10800	0.60588
3	0.67315	-0.30196	0.67286	-0.30556	0.04237	1.17771	0.61004
4	0.67279	-0.30177	0.67286	-0.30556	0.01043	1.24011	0.62527
5	0.67250	-0.30160	0.67286	-0.30556	0.05465	1.29520	0.67492

Then, if we compare the normalized error percentage trend between various types of angle of attacks with various wake model types, it is plotted as

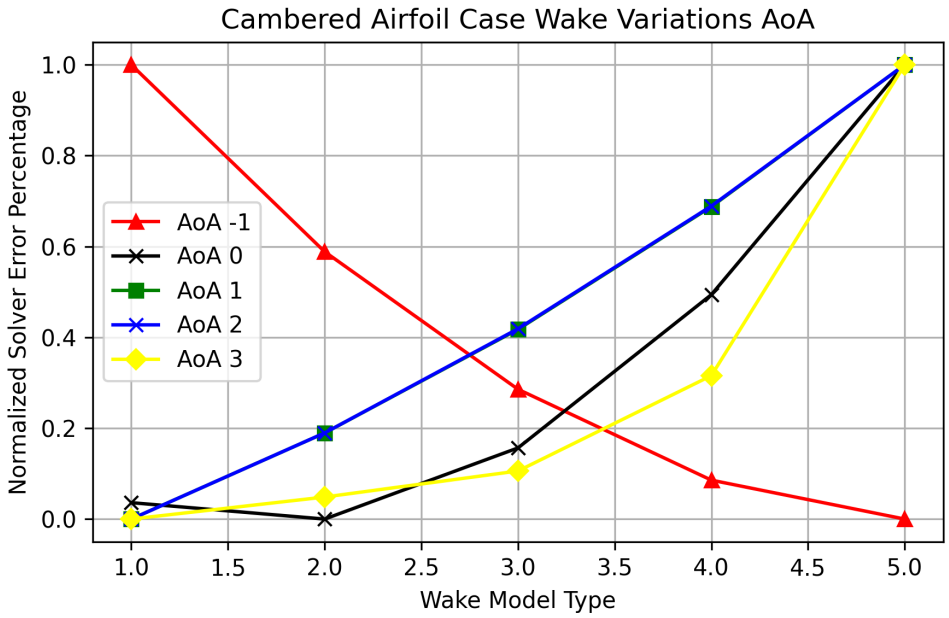

Figure 4.7: Cambered case wake model variations

From the plot, it could be seen that the general trend for zero to positive angle of attack, the error percentage lowers as the wake model is closer to the wake type model number 1, but for a negative angle of attack it behaves in the other direction where as the wake type model is closer to wake type model number 5, the error percentage lowers. Therefore, it could be said that the best wake model depends on how the free stream direction is towards the wing where the wake angle should follow the free stream incoming angle which is the angle of attack instead of opposing the direction to obtain a better wake model thus resulting in a lower error. The sense of direction of the free stream flow direction which is the angle of attack towards the wake model of number 1 to 5 could be seen as already illustrated in chapter 3.

4.3.2 Symmetrical Airfoil Case

This section presents the results of the panel method solver in a variety of wake models as described in chapter 3 for the symmetrical airfoil case compared to the XFLR5 solver.The results for the -1°to 3°angle of attack varied by the wake models respectively are as

Table 4.8: Symmetrical case AoA -1° wake variation results

Wake Model	Panel Method Solver		XFLR5 Solver		Error Percentage		
	CL	CM	CL	CM	CL Error %	CM Error %	Averaged Error %
1	-0.09237	0.02288	-0.09312	0.02337	0.80795	2.10727	1.45761
2	-0.09237	0.02288	-0.09312	0.02337	0.80797	2.10744	1.45771
3	-0.09237	0.02288	-0.09312	0.02337	0.80704	2.10635	1.45669
4	-0.09237	0.02288	-0.09312	0.02337	0.80514	2.10399	1.45456
5	-0.09237	0.02288	-0.09312	0.02337	0.80228	2.10037	1.45132

Table 4.9: Symmetrical case AoA 0° wake variation results

Wake Model	Panel Method Solver		XFLR5 Solver		Error Percentage		
	CL	CM	CL	CM	CL Error %	CM Error %	Averaged Error %
1	0.00000	0.00000	0.00000	0.00000	-	-	-
2	0.00000	0.00000	0.00000	0.00000	-	-	-
3	0.00000	0.00000	0.00000	0.00000	-	-	-
4	0.00000	0.00000	0.00000	0.00000	-	-	-
5	0.00000	0.00000	0.00000	0.00000	-	-	-

Table 4.10: Symmetrical case AoA 1° wake variation results

Wake Model	Panel Method Solver		XFLR5 Solver		Error Percentage		
	CL	CM	CL	CM	CL Error %	CM Error %	Averaged Error %
1	0.09237	-0.02287	0.09312	-0.02337	0.80938	2.12069	1.46504
2	0.09236	-0.02287	0.09312	-0.02337	0.81221	2.12422	1.46821
3	0.09236	-0.02287	0.09312	-0.02337	0.81408	2.12649	1.47028
4	0.09236	-0.02287	0.09312	-0.02337	0.81498	2.12749	1.47123
5	0.09236	-0.02287	0.09312	-0.02337	0.81493	2.12722	1.47107

Table 4.11: Symmetrical case AoA 2° wake variation results

Wake Model	Panel Method Solver		XFLR5 Solver		Error Percentage		
	CL	CM	CL	CM	CL Error %	CM Error %	Averaged Error %
1	0.18465	-0.04573	0.18619	-0.04671	0.82563	2.09657	1.46110
2	0.18463	-0.04572	0.18619	-0.04671	0.83697	2.11078	1.47388
3	0.18462	-0.04572	0.18619	-0.04671	0.84447	2.11994	1.48220
4	0.18461	-0.04572	0.18619	-0.04671	0.84813	2.12403	1.48608
5	0.18461	-0.04572	0.18619	-0.04671	0.84794	2.12308	1.48551

Table 4.12: Symmetrical case AoA 3° wake variation results

Wake Model	Panel Method Solver		XFLR5 Solver		Error Percentage		
	CL	CM	CL	CM	CL Error %	CM Error %	Averaged Error %
1	0.27676	-0.06855	0.27915	-0.06999	0.85498	2.06434	1.45966
2	0.27669	-0.06852	0.27915	-0.06999	0.88052	2.09640	1.48846
3	0.27664	-0.06851	0.27915	-0.06999	0.89741	2.11708	1.50725
4	0.27662	-0.06850	0.27915	-0.06999	0.90566	2.12638	1.51602
5	0.27662	-0.06850	0.27915	-0.06999	0.90528	2.12431	1.51479

Then, if we compare the normalized error percentage trend between various types of angle of attacks with various wake model types, it is plotted as

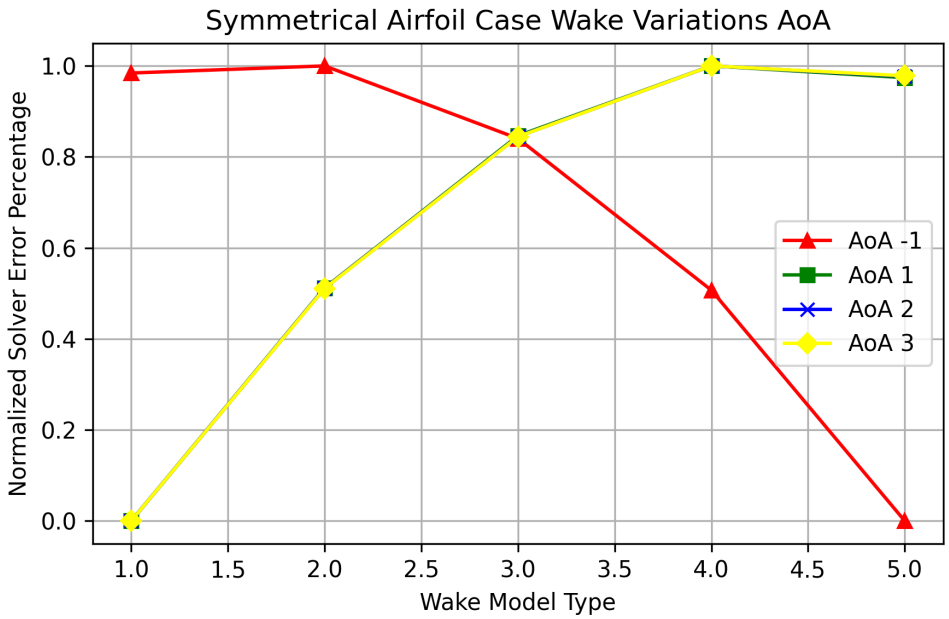

Figure 4.8: Symmetrical case wake model variations

Similarly to what could be seen from the analysis on the cambered airfoil case in section 4.2.1, the general trend for the symmetrical airfoil case is that for positive angle of attack the error percentage lowers as the wake model is closer to the wake type model number 1, but for a negative angle of attack it behaves in the other direction where as the wake type model is closer to wake type model number 5, the error percentage lowers. Therefore, this also leads to the statement that wake angle should follow the free stream incoming angle which is the angle of attack as a better wake model. Thus, picking the best wake model is also critical to obtain more accurate results where in the study cases of this work shows that using the right wake model could lower the error up to 0.07%.

4.4 Angle of Attack Variations

This section represents and analyzes how accurate is the panel method solver results compared to the results given by the XFLR5 solver in various angle of attacks that uses the wake model that provides the lowest error percentage as shown in chapter 4.2 before.

4.4.1 Cambered Airfoil Case

The results for the cambered airfoil case of the panel method solver compared to the results from the XFLR5 solver are as

Table 4.13: Cambered case angle of attack variations

AoA	Panel Method Solver		XFLR5 Solver		Error Percentage		
	CL	CM	CL	CM	CL Error %	CM Error %	Averaged Error %
-1	0.3024	-0.1920	0.3005	-0.1926	0.6284	0.3051	0.4668
0	0.3956	-0.2198	0.3940	-0.2210	0.4223	0.5465	0.4844
1	0.4886	-0.2474	0.4872	-0.2493	0.2894	0.7600	0.5247
2	0.5815	-0.2749	0.5802	-0.2775	0.2200	0.9131	0.5666
3	0.6740	-0.3024	0.6729	-0.3056	0.1737	1.0310	0.6024

The direct comparison of the lift coefficient and moment coefficient results between solvers are plotted as

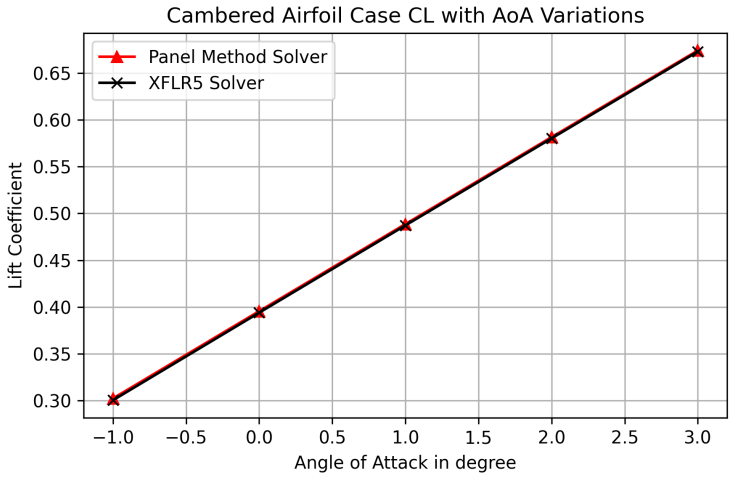

Figure 4.9: Cambered case CL with AoA variations

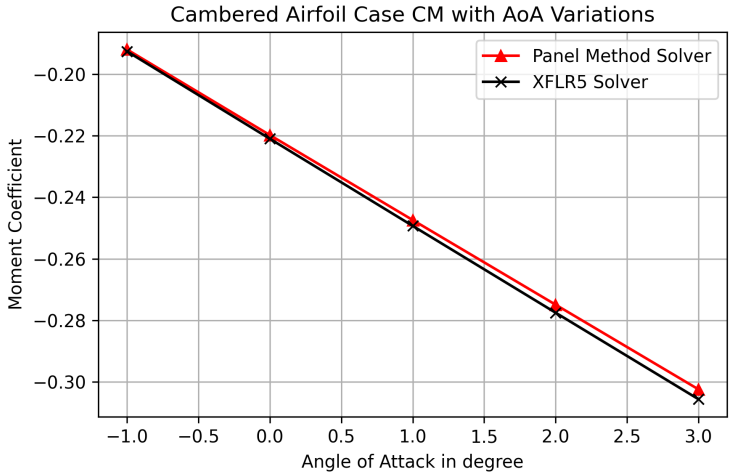

Figure 4.10: Cambered case CM with AoA variations

The results show that generally the panel method solver proposed by this work could provide good results to predict lift and the moment coefficient compared to the XFLR5 software with an averaged error of around 0.5%, but it is also noted that as the angle of attack increases where separation phenomena should start to happen, the error of the solver compared to the XFLR5 solver would increase as it is not modeled in the panel method solver

by assumptions.

4.4.2 Symmetrical Airfoil Case

The results for the symmetrical airfoil case of the panel method solver compared to the results from the XFLR5 solver are as

Table 4.14: Symmetrical case angle of attack variations

AoA	Panel Method Solver		XFLR5 Solver		Error Percentage		
	CL	CM	CL	CM	CL Error %	CM Error %	Averaged Error %
-1	-0.0924	0.0229	-0.0931	0.0234	0.8023	2.1004	1.4513
0	0.0000	0.0000	0.0000	0.0000	-	-	-
1	0.0924	-0.0229	0.0931	-0.0234	0.8094	2.1207	1.4650
2	0.1847	-0.0457	0.1862	-0.0467	0.8256	2.0966	1.4611
3	0.2768	-0.0685	0.2791	-0.0700	0.8550	2.0643	1.4597

The direct comparison of the lift coefficient and moment coefficient results between solvers are plotted as

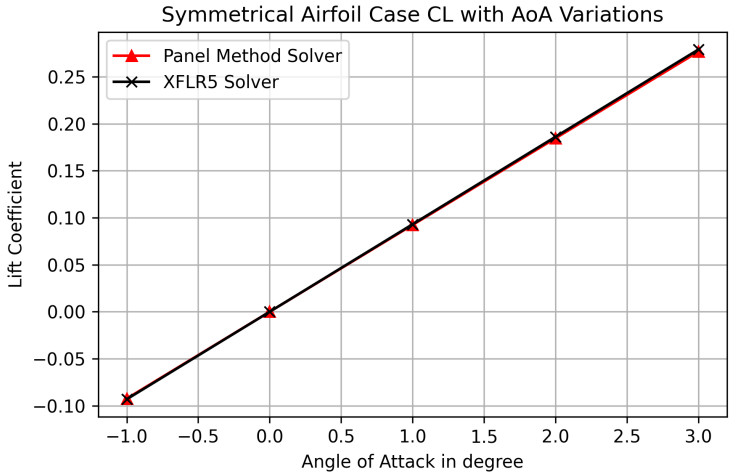

Figure 4.11: Symmetrical case CL with AoA variations

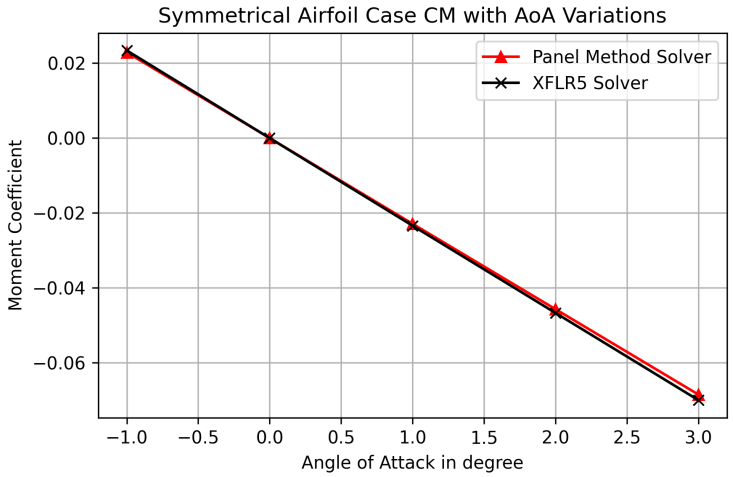

Figure 4.12: Symmetrical case CM with AoA variations

Similarly to the cambered airfoil case, the results show that generally the panel method solver proposed by this work could provide good results to predict lift and the moment coefficient compared to the XFLR5 software with an averaged error of around 1.45% for the symmetrical airfoil case, but also similarly to the cambered airfoil case it is also noted that as the angle of attack increases where separation phenomena should start to happen, the error of the solver compared to the XFLR5 solver would increase as it is not modeled in the panel method solver by assumptions.

Chapter 5

Conclusions

5.1 Concluding Remarks

From the results shown in the previous chapters, some conclusions that could be obtained are

1. This work has implemented a panel method based solver to calculate the pressure distribution around a three-dimensional wing and the aerodynamics force coefficients could be calculated.

2. The proposed solver is able to perform calculations for two types of wing test cases where the first case involves a cambered airfoil wing with sweep and the second case uses a symmetrical airfoil wing without sweep and results in satisfyingly accurate results at an averaged error of 0.5% for the first case and 1.45% for the second case when compared to the well-established XFLR5 solver.

3. The wake model or wake angle at the trailing edge were found to be depending on the angle of attack where the wake angle tends to follow the direction of the free stream flow resulting in different directions for

positive and negative angle of attack cases and by using the preferable and correct wake model could lower the error for up to 0.07%.

4. The proposed solver could provide accurate results in low angle of attack where from the results there are noticeable increase in error as the angle of attack increases. This is due to the limitations of panel method that was assumed not able to model rotational flows where as the angle of attack increases, flow separation would need to be modeled.

5.2 Future Works

Some future works to improve on this project are as

- Combining the panel method with boundary layer modeling and turbulent flow models.
- Perform an automated wake angle finding algorithm on a more complex wake model that could be based on the wake model recommendations proposed from this work's results.
- Using higher order panel such as second order polynomial.

Bibliography

[1] J. Katz and A. Plotkin, *Low-speed aerodynamics*, vol. 13. Cambridge university press, 2001.

[2] B. Maskew, "Program vsaero theory document: a computer program for calculating nonlinear aerodynamic characteristics of arbitrary configurations," 1987.

[3] J. L. Hess and A. O. Smith, "Calculation of potential flow about arbitrary bodies," *Progress in Aerospace Sciences*, vol. 8, pp. 1–138, 1967.